

# Decorated vertex with 3-edged cells in 2D foams: exact solutions and properties.

M. Mancini<sup>1a</sup> and C. Oguey<sup>2</sup>

<sup>1</sup> G M C M , CNRS U M R 6626, Université de Rennes I-35042 Rennes cedex, France.

<sup>2</sup> LPTM , CNRS U M R 8089, Université de Cergy-Pontoise, 95031 Cergy-Pontoise, France.

v3.5 May 25, 2019/ Received: date/ Revised version: date

**Abstract.** The energy, area and excess energy of a decorated vertex in a 2D foam are calculated. The general shape of the vertex and its decoration are described analytically by a reference pattern mapped by a parametric Möbius transformation. A single parameter of control allows to describe, in a common framework, different types of decorations, by liquid triangles or 3-sided bubbles, and other non-conventional cells. A solution is proposed to explain the stability threshold in the corner problem.

**PACS.** 82.70.Rr *Aerosols and foams* { 82.70.Kj *Emulsions and suspensions* { 68.03.Hj *Gas-liquid and vacuum-liquid interfaces: Structure, measurements and simulations*

## 1 Introduction

Since J. P. Laveau [1], 2D foams have been extensively studied, experimentally and theoretically, because they are simpler than three-dimensional systems [2].

In the dry model of 2D soap foams, the gas is assumed incompressible and the liquid fraction is assumed vanishing. Although the dry model correctly describes some aspects of foam physics like energy minimization, equilibrium configurations, etc [2], in many other cases, the presence of the liquid needs to be taken into account, both theoretically [3] and to match experimental observations [4,5,6].

The more realistic model of foams, including a small liquid fraction at the nodes, is related to the dry model by Waeire's decoration theorem. The decoration theorem [7] and, later, the star-triangle theorem [3] state that, in 2D foams, the lines connecting a 3-sided cell, Plateau border or bubble, if continued inside the cell, all intersect at a single point and satisfy the equilibrium conditions (Fig. 1). Conversely, it is always possible to decorate a 3-fold vertex at equilibrium by a Plateau border or a 3-sided bubble. The decoration theorem validates the ideal dry model for slightly wet foams as far as equilibrium is concerned [2]; the star-triangle equivalence permits, in principle, to take away 3-sided bubbles in searching equilibrium configurations. Notice, however, that the foam energy, the area of the bubbles, coarsening and most mechanical properties of the foam change if the decoration is switched on or off.

In most quasi-static transformations, the foam dynamics is driven by energy minimization at fixed bubbles area. So knowing the energy and areas is an important issue [8].

In this paper, we calculate the energy of a wet-decorated foam starting from the energy of the dry model.

Recently, Teixeira and Fortes [9] gave the equations describing the exact geometry of a general Plateau border with zero disjunction pressure ( $\gamma_{\text{border}} = \frac{1}{2} \gamma_{\text{m}}$ ), calculating the excess energy among other quantities. The excess energy is the energy difference between a decorated and a dry vertex.

Using the invariance of 2D foams under Möbius transformations [10], we generalise this problem to the cases where the surface tension of the lines and that of the decorating triangles are arbitrary, giving the Plateau border and 3-sided bubble problems a unified description. We calculate the excess energy  $E$  and all geometrical quantities as a function of four parameters which characterise the cluster size and shape. Normalising the excess energy by the square root of the triangle area gives a scale-invariant quantity, the excess energy density:

$$= E = \frac{p}{A} :$$

In realistic foams, the excess energy density of 3-cells is a line in  $A$  with a good approximation:

$$(A) \propto b + bA;$$

where  $b$  depends on the form of the decorated lines. According to Lewis' law [11], the average cell area increases linearly with the number of sides or neighbours:  $A_n \propto n$ . So the triangle area  $A_3$  is small on average. As we'll see, the slope  $b$  is proportional to the sum of the squared curvature of the lines meeting at the decorated vertex; being zero in the 3-fold symmetric case,  $b$  measures the deviation from perfect symmetry.

<sup>a</sup> e-mail: marco.mancini@univ-rennes1.fr

In the final part, we apply our analytical results to the corner problem. Experimentally, a bubble spontaneously gets out [5] before the critical area is reached where the dry model predicts a spontaneous symmetry reduction [12]. Following the experimentalists suggestion that the ejection might be due to the presence of liquid, we solve the problem by including liquid triangles around the vertices and calculating a threshold area for the central bubble at which two vertices get into contact. Our conjecture is that this contact triggers the ejection.

## 2 Equilibrium of 2D foams

In equilibrated 2D dry foams, the bubbles are separated by lines obeying the Laplace-Young law:

$$P + k = 0 \quad (1)$$

$P = P_2 - P_1$  is the pressure difference across the line, the surface tension and  $k$  the curvature of the line [2]. In static conditions and in absence of applied field, the pressure inside each bubble is constant so that the lines are arcs of circle.

The lines meet three by three at vertices in a manner satisfying Plateau's laws [1,2]:

$$\sum_{j=1}^3 \mathbf{t}_j = 0; \quad (2)$$

$$\sum_{j=1}^3 \mathbf{k}_j = 0; \quad (3)$$

where  $\mathbf{t}_j$  is the unit vector tangent to the line at the vertex and where the surface tension,  $\gamma_j$  ( $j > 0$ ), may differ from line to line [3,13,14,15].

These equations should be understood as pertaining to general cellular systems with surface tensions; bubbles may be gas or liquid cells, including Plateau borders, and lines mean boundary edges, either bi-layers or liquid-gas interface.

The symmetry group of 2D foams at equilibrium is the group of homographies, or Möbius maps, generated by Euclidean similarities and inversion [13,16]. Some definitions and basic properties of Möbius maps are recalled in appendix A.

Equations (2) and (3) also imply that the centres of the three circular edges meeting at a vertex are aligned [13].

The energy of a 2D bubble cluster is the sum, over the set of edges  $j$ , of the edge length,  $l_j$ , weighted by surface (line in 2D) tension:

$$E = \sum_j l_j \gamma_j$$

### 2.1 Star-Triangle Equivalence

The pressure and the surface tensions fix the triangle geometry. In a standard dry equilibrated 2D foam, where the surface tension is constant overall the foam ( $\gamma_j = \gamma$ ), the

triangles are convex 3-sided bubble. If a slight amount of liquid is added to the foam, it is mainly confined around the vertices, in Plateau borders forming concave triangles.

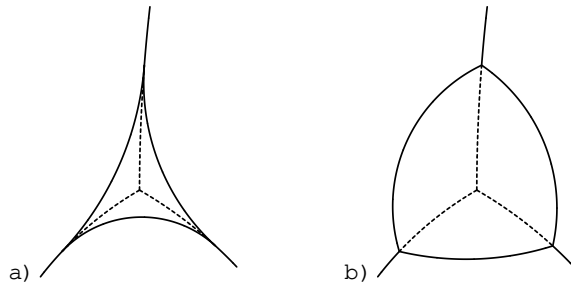


Fig. 1. Star-triangle equivalence. a) Decoration by a liquid triangle. b) Equivalence of a star and a 3-sided bubble.

In the star-triangle equivalence, the star is an equilibrated figure formed by a vertex and the three edges meeting at it [3]. When we consider a triangle and its associated star as a whole, a star+triangle, we will call it 3-cell.

The star-triangle equivalence was proved in full generality for cellular systems with multiple surface tensions ( $j \in j_0$ , non-standard foams) [3]. The star-triangle equivalence implies Weaire's decoration theorem [7] by triangular Plateau borders (fig. 1-a) when the surface tensions of the triangle sides are those of a liquid-gas interface,  $\gamma_e$  cell =  $\gamma_g$ , while the star has the line surface tension:  $\gamma_i = \gamma_m / 2 \gamma_g$ . For a standard 3-sided bubble, star-triangle equivalence involves the same tension everywhere:  $\gamma_i = \gamma_e = \gamma_m$ .

In 3 dimensions, a decoration-bubble theorem holds only for spherical foams [17]. When the lines are not necessarily spherical, Teixeira and Fortes proposed a modified version involving both line and surface tensions [18].

## 3 Conformal description of the 3-cell

Starting from a two-parameter reference 3-cell, we obtain a general 3-cell by a Möbius transformation.

To fix notations, let ' $^{ex}$ ', of radius  $r^{ex}$ , be the external (or decorating) edges, and ' $^{in}$ ', of radius  $r^{in}$ , the internal (decorated) ones. When the central vertex  $v_0$  is decorated by a triangle,  $v_0$  and the portion of ' $^{in}$ ' interior to the triangle are virtual. Conversely, when the central vertex is not decorated, the ' $^{ex}$ ' are virtual. We will use the convention of signed angles and radii, in a way such that the arc length is always positive [7].

In this paper, we allow only two different values for  $\gamma$ : the surface tension of the external lines or interfaces, on the triangle sides, is  $\gamma_e$ , and that of internal lines, on the star edges, is  $\gamma_i$ . These tensions are related by equation (2), applied to a vertex of the triangle:

$$\gamma_i = 2 \gamma_e \cos \alpha \quad (4)$$

The contact angle is the angle between  $\ell^{\text{in}}$  and  $\ell^{\text{ex}}$ .

If the thickness of the films,  $h$ , is not negligible, the angle is related to the disjunction pressure [14,15,17]:

$$=\frac{i}{h}(\cos 1):$$

The excess energy is the energy gained by decorating the vertex. It is the difference of the internal and external edge lengths, weighted by the surface tensions [9]:

$$E = E_{\text{triangle}} - E_{\text{star}} = \frac{e^{\text{ex}} - e^{\text{in}}}{i} L^{\text{in}}$$

$$= \frac{L^{\text{ex}}}{i} - \frac{L^{\text{in}}}{2 \cos(\alpha + \frac{\pi}{6})} : \quad (5)$$

The excess energy density is defined as the ratio of the excess energy  $E$  over the square root of the triangle area:

$$\frac{E}{A_{\text{triangle}}^{1/2}} : \quad (6)$$

From now on, we will set  $i = 1$ ; the surface tension of the internal films is our tension unit.

### 3.1 The reference 3-cell

The reference 3-cell  $C(q)$ , of parameters  $q$  and  $q$ , is defined in figure 2. It is symmetric.

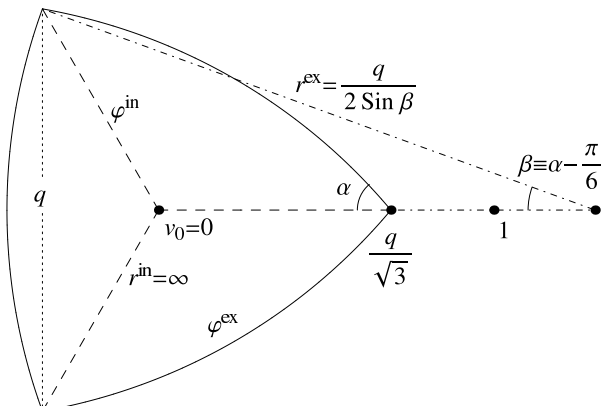


Fig. 2. Symmetric 3-cell with parameters  $q$  and  $q$ . The star (internal films) is represented by dashed lines.

The parameter  $q \neq 0$  is the chord length of the curved sides of the reference triangle. It specifies the triangle size.

The angle is related to the contact angle by

$=6$ . As conformal means angle preserving, and are preserved by the Möbius transformation applied to, or from, the reference cell. Choosing  $\beta$ , rather than  $\alpha$ , helps in treating Plateau borders and 3-sided bubbles in a common way. In figure (1-a),  $\beta$  is equal to  $=6$ ; in fig. (1-b),  $=6$ . For the reference cell, the angle subtended by the external edges equals  $2\pi$ ; this property is not generally preserved by conformal transformations.

When  $=3$ ,  $i = e = 0$  and the sides of the triangle  $C(q)$  form a circle. This case describes a 3 cells partition of a disc surrounded by a rigid membrane. So, the interpretation of the 3-cell as a bubble or a liquid drop is limited to the values  $2$  [ $=6; =3$ ].

The edge curves are parametrised by

$$\ell_j^{\text{in}}(t_1) = e^{i_j} t_1; \quad \text{with } t_1 \in [0; \frac{\pi}{3}]; \quad (7)$$

$$\ell_j^{\text{ex}}(t_2) = \frac{qe^{i_j}}{2 \sin(\beta)} \frac{2}{3} \cos(\beta + \frac{\pi}{6}) e^{i_j} t_2; \quad (8)$$

with  $t_2 \in [0; 1]$ .  $j = 1, 2, 3$  indexes the edges and  $j = 3$ .

The curve (8) depends continuously on  $\beta$  [ $=6; =3$ ]. Its curvature vanishes, and changes sign, at  $\beta = 0$ . The equilateral triangle is curved, convex, at positive  $\beta$ ; curved, concave, at negative  $\beta$ ; and it has straight edges at  $\beta = 0$ . At  $\beta = 0$  the parametrisation is given by the limit of (8) as  $\beta \rightarrow 0$ :

$$\ell_j^{\text{ex}}(t_2) = q e^{i_j} \frac{1}{2} \sqrt{3}^{1/2} + i t_2 : \quad (9)$$

With (4) and (5), the excess energy of the reference cell is

$$E(q) = \frac{3}{2 \sin(\beta + \frac{\pi}{6})} \frac{p}{3} q : \quad (10)$$

The triangle area is the sum of the area,  $A_4$ , of the rectilinear equilateral triangle formed by the external vertices, and  $A_1$ , the signed area of the three lenses around the straight triangle:

$$A(q) = A_4 + A_1 = \frac{p}{4} \frac{3}{4} + \frac{3}{8} \frac{2}{\sin^2(\beta)} \frac{\sin(2\beta)}{\sin(2\beta)} q^2 : \quad (11)$$

Finally, the reference excess energy density is obtained by dividing the excess energy by the area square root:

$$\sigma^0 = \frac{E(q)}{A(q)^{1/2}} = \frac{q}{\sqrt{3}} \frac{p}{2 \sqrt{3} \cos(\beta + \frac{\pi}{6}) \sin(\beta)} = \text{sign}(\beta) \frac{q}{\sqrt{\cos(\beta + \frac{\pi}{6})}} : \quad (12)$$

Being scale invariant,  $\sigma^0$  does not depend on  $q$ . In the particular cases of a Plateau border and of an equal 3-sided bubble, the respective  $\sigma^0$  are

$$\sigma^0_{=6} = \frac{q}{\sqrt{3}} \frac{p}{2} = 2, \quad 0.401565;$$

$$\sigma^0_{=3} = \frac{q}{2} \frac{p}{3} = 1.67901 :$$

Notice that the reference star is fixed, with standard Plateau angles  $2\pi/3$ , independent of the parameters  $q$  and  $\beta$ .

### 3.2 The general 3-cell

Applying a suitable Möbius transformation to the reference 3-cell, produces a general 3-cell compatible with our assumptions.

Given a star, the decorating triangle is entirely specified by its area  $A$  and contact angle  $\beta$ ; those will be related to the parameters  $q$  and  $s$  of the reference 3-cell. In the star, centred at vertex  $v^0$ , the three (internal)  $\text{Im } s = 1, 2, 3$  have curvature  $k_i$ . Because of equation (3), only two of the curvatures are independent. So we need only a one-complex parameter Möbius transformation to reach all possible star+triangle figures.

A general Möbius transformation  $f$ , given by (42), has six real parameters, much beyond our needs. We require that the transformation preserves orientation, that it maps the interior of the reference 3-cell onto the interior of the general 3-cell. In addition, we can fix a length scale, the central vertex position, and one of the  $\text{Im } s$  tangents there (by conformality, this fixes all the tangents at  $v^0$ ). Choosing the origin at  $v^0$ , this means  $f(0) = 0$  and  $f'(0) > 0$ . Then the Möbius transformation can be written in the form

$$f_s(z) = (1 - \beta j) \frac{z}{1 - sz}; \quad \text{with } \beta j = ss < 1; \quad (13)$$

depending on the single complex parameter  $s$ . The result is a 4 (real) parameter star+triangle figure:  $\mathcal{C}(s; q; \beta)$  =  $f_s(C(q; \beta))$ . We designate the transformed quantities by a tilde (appendix A). An example is given in figure 3.

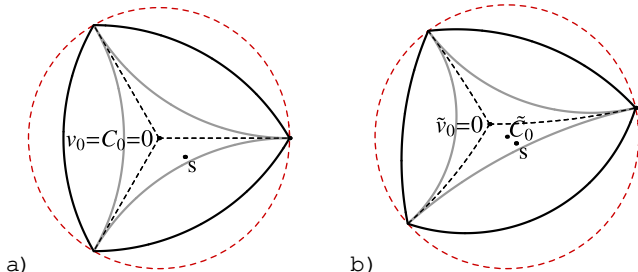


Fig. 3. a) The reference 3-cell  $C(q; \beta)$ ,  $\beta = 6$  (in black) and  $\beta = 6$  (in grey). b) General 3-cell  $C(s; q; \beta)$ , in image of a) by  $f_s$ . The figures are calculated for  $q = \frac{1}{2}$  and  $s = 0.2 \exp(-i\pi/5)$ . The circumscribed circle in b) is given by (14).

The points  $z = 0$  and  $s$  are fixed points of  $f_s$ . The complex function  $f_s$  maps the reference circumscribed circle, of centre  $C_0 = v_0 = 0$  and radius  $r_0 = q = \frac{1}{3}$  (fig. 3), onto the circle of parameters (eq. (43)):

$$(C_0; r_0) = q^2 \frac{s(1 - \beta j)}{3 - q^2 \beta j}; q \frac{p}{\beta} \frac{3(1 - \beta j)}{q^2 \beta j} : \quad (14)$$

The 3-cell is contained in the disc  $(C_0; r_0)$  for  $\beta j < \frac{1}{3}$ , while it is outside<sup>1</sup> the disc for  $\beta j > \frac{1}{3}$ .

<sup>1</sup> This peculiar situation is possible only when the triangle is curved and has two concave sides.

As the equilibrium equations (2) and (3) are left invariant by  $f_s$ , the image of the reference cell is in mechanical equilibrium.

In order to get physically meaningful patterns,  $q$  must be bounded:  $q < q_{\max}(s; \beta)$ . An expression for  $q_{\max}(s; \beta)$  will be derived in section 4.1. Here, we just give its origin and meaning. At  $q = q_{\max}$ , the reference boundary,  $\partial C(q; \beta)$ , meets  $1=s$ , the pole of  $f_s$ ; this condition defines  $q_{\max}(s; \beta)$ . When  $q < q_{\max}$ , the reference triangle is mapped to a bounded triangle but, when  $q > q_{\max}$ , the reference interior is mapped to the exterior of the triangle boundary, of infinite area, violating our requirements.

The divergence at  $q = q_{\max}$  is illustrated in figure 4. First, recall that any equilibrated star vertex has a

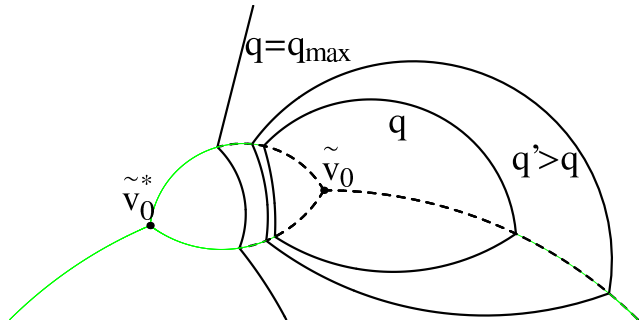


Fig. 4. Two different 3-cells  $C(s; q; \beta)$  calculated for  $\beta = 6$ ,  $q$  and  $q^0$ , with  $q^0 > q$ . The continuation of the internal  $\text{Im } s$  is plotted in grey (green on-line).

conjugate  $v^*$  where the circles supporting the star edges also meet. The position of  $v^*$  is the mirror reflection of  $v_0$  through the line of the curvature centres [13,17]. For the reference  $C(q; \beta)$ , the conjugate of  $v_0 = 0$  is  $v_0 = 1$ ; in  $\mathcal{C}(s; q; \beta)$ ,  $v_0$  is given by

$$v_0 = f_s(1) = s(\beta j)^2 - 1 : \quad (15)$$

By increasing  $q$  alone, the triangle vertices move along the star edges, towards infinity in the reference, and so, towards  $v_0$  under the mapping  $f_s$  (figure 4). When  $q = q_{\max}$ , the triangle area is infinite and all the edge radii are negative.

In real foam  $s$ , where the star edges end at neighbour vertices, the divergence is not reached. Topological changes screen this phenomenon.

### 3.3 Extension to special 3-cells

Although the 3-cell is well defined only for values  $\beta = 3$ , the equations can be extended, for particular values of the parameters, to cover other physical or mathematical situations.

#### 3.3.1 Case $\beta = 3$

As noticed in sec. 3.1, the reference  $C(q; \beta = 3)$  is a disc.  $f_s$  maps it to a disc divided into three bubbles by  $\text{Im } s$

meeting the outer boundary orthogonally<sup>2</sup>. Carstea and Ritore [19] proved that this type of graph is the unique least-perimeter way of partitioning the unit disk into three regions of prescribed areas.

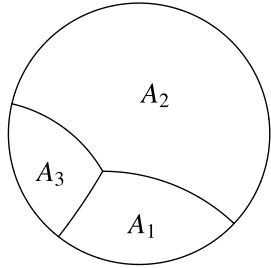


Fig. 5. For  $q = \frac{p}{3}$  and  $\beta = 3$ , varying  $s$ , the star describes all the least-perimeter partitions of the unit disk into three regions of prescribed areas.

### 3.3.2 Case $\beta = 2$

When  $\beta = 2$ , considering  $r^{\text{in}}$  and  $r^{\text{ex}}$  as real in  $s$ , the graphics of the reference 3-cell is equivalent to a symmetric three bubble cluster<sup>3</sup> (figure 6-a). The absolute value of (12) gives its energy density ( $E = \langle A \rangle$ ):

$$s = j^0 = \frac{q}{4 \beta^2} = \frac{q}{4 \cdot 3 + 6} = 5.07718;$$

Applying (13) to the reference produces a general three bubble cluster (figure 6-b).

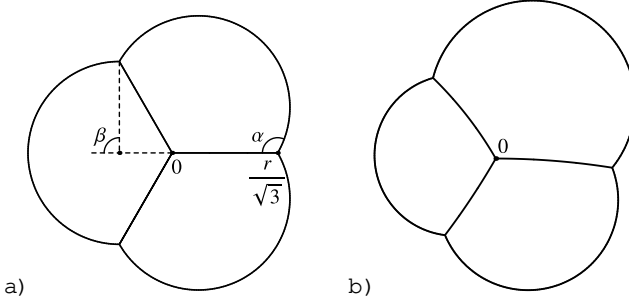


Fig. 6. a) At  $\beta = 2$ , the reference describes a cluster of 3 identical bubbles. b) Three-bubble cluster transformed by  $f_s$ .

## 4 Area and energy of a general 3-cell

To calculate the excess energy density of a 3-cell  $\mathcal{C}(s; q; \beta)$ , we need to calculate its external and internal perimeter, its area and its edge curvatures.

<sup>2</sup>  $\beta = 2$  is the angle formed by the soap film with a rigid wall or membrane.

<sup>3</sup> Interpreted, here, as an inverted triangle lying around the cluster.

Let us start with the edge radii. Using equations (43) and (44), they are, for  $j = 1; 2; 3$ ,

$$r_j^{\text{in}} = \frac{1}{2 \beta j \sin(\frac{j}{3} \pi)}; \quad (16)$$

$$r_j^{\text{ex}} = \frac{6 \cdot 1 \cdot \beta^2 \cdot r \sin}{4 \beta^2 \sin q \sin^2 \frac{j}{3} \pi \cos(\frac{j}{3} \pi) + 3q^2 \beta^2}; \quad (17)$$

where  $s = \arg(s)$ . As expected, the radii  $r^{\text{in}} = r^{\text{in}}(s)$  don't depend on  $q$ . The radii inverse, that is, the curvatures, verify the equilibrium equations (3), and the following ones:

$$K_{\text{in}}^2(\beta) \sum_{j=1}^{X^3} \frac{1}{(r_j^{\text{in}})^2} = 6 \cdot \frac{\beta^2}{1 - \beta^2}^2; \quad (18)$$

$$K_{\text{ex}}^2(\beta) \sum_{j=1}^{X^3} \frac{1}{(r_j^{\text{ex}})^2} = \frac{8 \beta^2 \cos^2(\frac{j}{3} \pi)}{(1 - \beta^2)^2} + \\ + \frac{4 \beta^2 q^2 \cos(\frac{j}{3} \pi) - 3 \sin^2}{3(1 - \beta^2)^2 q^2}; \quad (19)$$

Thus, the sum of the squared curvatures, internal or external, doesn't depend on the argument of  $s$ . Eq. (18) even states that the internal sum depends only on  $\beta$ .

### 4.1 Perimeters

The value of the internal perimeter  $\Gamma^{\text{in}}(s; q)$  follows from a straightforward calculation detailed in appendix B.

$$\Gamma^{\text{in}}(s; q) = \sum_{j=1}^{X^3} \ell_j^{\text{in}} = \sum_{j=1}^{X^3} r_j^{\text{in}}(s) \cdot \psi_j^{\text{in}}(s; q); \quad (20)$$

where

$$\psi_j^{\text{in}}(s; q) = 2 \arctan \frac{3^{1/2} q \beta j \cos(\frac{j}{3} \pi) - s}{\sin(\frac{j}{3} \pi)} + \\ + 2 \arctan \frac{\cos(\frac{j}{3} \pi)}{\sin(\frac{j}{3} \pi)} \quad (21)$$

is the (signed) angle subtended by the internal in  $\ell_j^{\text{in}}$ .

The internal perimeter  $\Gamma^{\text{in}}$  doesn't depend on  $s$ .

Analogously, the external perimeter is given by:

$$\Gamma^{\text{ex}}(s; q) = \sum_{j=1}^{X^3} \ell_j^{\text{ex}} = \sum_{j=1}^{X^3} r_j^{\text{ex}}(s; q; \beta) \cdot \psi_j^{\text{ex}}(s; q; \beta) \quad (22)$$

where  $\psi_j^{\text{ex}}(s; q; \beta)$  is the angle subtended by the external edge  $\ell_j^{\text{ex}}$ , defined by (53). The angles  $\psi_j^{\text{ex}}$  verify the equation

$$\sum_{j=1}^{X^3} \psi_j^{\text{ex}} = 6; \quad (23)$$

consequence of the fact that the angles of the (rectilinear) triangle sum up to (see figure 7).

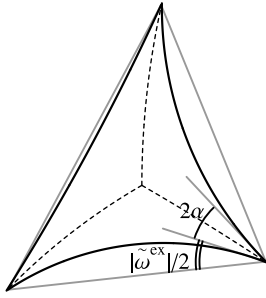


Fig. 7. Star and triangle for  $\alpha = 10^\circ$ . Summing the internal angles of the grey triangle gives (23).

The limit value  $q_{\max}(s; \alpha)$  (section 3.2), where the boundary of the reference triangle meets the pole  $1=s$  of  $f_s$ , can be derived from (17). Indeed, fixing all the parameters ( $s$  and  $\alpha$ ) but  $q$ , the sign of  $k_j = 1-r_j^{\text{ex}}$  changes when the circle supporting  $r_j^{\text{ex}}$  meets the pole  $1=s$ . For each  $j = 1, 2, 3$ , this occurs at the positive solution  $q = q_j$  of

$$k_j = 1-r_j^{\text{ex}}(s; q; \alpha) = 0; \quad (24)$$

The explicit expression of  $q_j$  is:

$$q_j(s; \alpha) = \frac{\frac{p}{3} \left( 3 - 4 \cos^2 \left( \alpha + \frac{\pi}{6} \right) \sin^2 \left( \frac{j\pi}{3} - s \right) \right)^{1/2}}{2\beta_j \cos \left( \frac{\pi}{6} \right)} \frac{p}{3 \cos \left( \alpha + \frac{\pi}{6} \right) \cos \left( \frac{j\pi}{3} - s \right)} \frac{\beta_j \cos \left( \frac{\pi}{6} \right)}{; \quad (25)}$$

When  $q$  increases, the pole is first met by circle portions outside the triangle. The bound  $q = q_{\max}(s; \alpha)$  corresponds to the encounter with the triangle boundary in the last of the three circles:

$$q_{\max}(s; \alpha) = \max_{j=1,2,3} q_j; \quad (26)$$

For  $q > q_{\max}$ , the interior of the 3-cell is no more bounded and relation (23) is no longer verified, as illustrated on fig. 4.

## 4.2 Area

The area of the 3-cell  $\mathcal{C}(s; q; \alpha)$  is the sum of four parts: the rectilinear triangle based on the external vertices and the (signed) area of the three lenses around:

$$\mathcal{A}(s; q) = \mathcal{A}_4(s; q) + \mathcal{A}_{\text{ext}}(s; q); \quad (27)$$

with

$$\mathcal{A}_4 = 2 r_1^{\text{ex}} r_2^{\text{ex}} \sin \frac{k_1}{2} \sin \frac{k_2}{2} \sin \frac{\pi}{3} + \frac{k_3}{2}; \quad (28)$$

$$\mathcal{A}_{\text{ext}} = \frac{1}{2} \sum_{j=1}^3 (r_j^{\text{ex}})^2 (\beta_j - \sin \beta_j); \quad (29)$$

Although  $\alpha$  appears in the RHS of (28), it is clear that the area of the triangle  $\mathcal{A}_4$  doesn't depend on it. Indeed, the triangle 4 is built only on the vertices, independent of  $\alpha$  (they are determined by  $q$  in the reference and then mapped by  $f_s$ ).

## 4.3 Excess energy density

Using (20), (22) and (27) we obtain the excess energy density for a general 3-cell  $\mathcal{C}(s; q; \alpha)$ :

$$(s; q) = \frac{\mathcal{E}^{\text{ex}}(s; q) = (2 \cos(\alpha + \pi/6)) \mathcal{E}^{\text{in}}(s; q)}{\mathcal{A}(s; q)^{1/2}}; \quad (30)$$

Before we draw the plots, let us make a change of variables to take advantage of the scale invariance of the excess energy density, already noticed. The new parametrization is defined as follows:

$$\begin{aligned} \zeta &= q(1 - \beta_j^2) \quad \text{with} \quad \zeta \geq 0; \\ \beta_j &= q \beta_j \quad \text{with} \quad 0 \leq \beta_j \leq \pi/3; \\ \theta_s &= \arg(s); \end{aligned} \quad (31)$$

where  $(\zeta; \theta_s) = (\beta_j; \theta_s)$  is independent of  $\beta_j$  by (25). The fourth parameter,  $\alpha$ , is unchanged. The parameter corresponds to a magnification of the 3-cell, so the excess energy density doesn't depend on it. Moreover, from the symmetry of the reference 3-cell under the group  $D_3$  generated by mirrors at  $\alpha = 30^\circ$ , the excess energy density verifies:

$$(\zeta; \theta_s) = (\zeta; \frac{2}{3} - \theta_s); \quad (32)$$

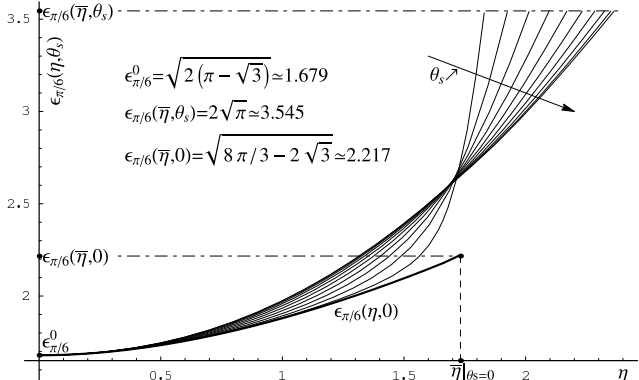


Fig. 8. Plot of the excess energy density of a 3-sided bubble ( $\alpha = 60^\circ$ ) as a function of  $\zeta = q\beta_j$  for some values of  $\theta_s$  ( $\alpha = 30^\circ$ ). The solid line corresponds to  $\theta_s = 0$  where the system has a mirror symmetry. The dot-dashed lines point out the limit values of  $\zeta$  calculated at  $\alpha = 60^\circ$ .

Figures 8 and 9 show the plots of  $(\zeta; \theta_s)$  for a 3-sided bubble and a plateau border, respectively. In both cases, the excess energy density is minimal for  $\zeta = 0$ , i.e. in the symmetrical reference configuration.

In the 3-sided bubble case, for low values of  $\zeta$ ,  $\zeta = 6$  increases with  $\theta_s$  while, for greater  $\zeta$ , it decreases with  $\theta_s$ ; the change,  $(\zeta = \zeta_s)$  ( $\zeta = 6$ ;  $\zeta = 0$ ) occurs at values close to  $(\zeta = 6; \theta_s = 0)$ . At  $\zeta = (\zeta = 6; \theta_s = 0)$ ,  $\zeta = 6$  ( $\zeta = 6; \theta_s = 0$ ) is constant as a function of  $\theta_s$ , meaning that all the curves in fig. 8 end at the same ordinate.

In the plateau border ( $\alpha = 60^\circ$ ),  $\zeta = 6$  is a non-increasing function of  $\theta_s$ :  $(\zeta = \zeta_s)$  ( $\zeta = 6$ ;  $\theta_s = 0$ ). For any  $\theta_s$ , at

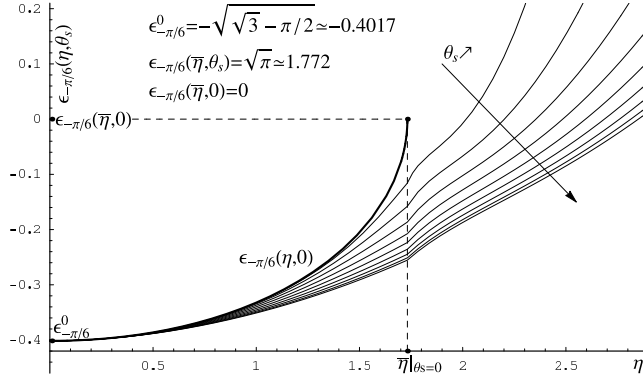


Fig. 9. The excess energy density of a Plateau border ( $\gamma = 6$ ) as a function of  $\eta = q_s \theta_s$  for some values of  $0 < \theta_s < 3$ . The solid line corresponds to  $\theta_s = 0$ , where the border has a mirror symmetry.

$\gamma = 0$ , the external vertices stay on a line and the area of the rectilinear triangle is zero:  $\mathcal{A}_4 = 0$ . This implies that at  $\gamma = 0$ , the derivative  $(\partial/\partial \eta) \epsilon_{-6}$  has a singularity, corresponding to the cuspidal points of  $\epsilon_{-6}(\eta; \theta_s)$  in figure 9. Again, in this case, at  $\gamma = (6; \theta_s)$  and  $\theta_s \neq 0$ , the excess energy density doesn't depend on  $\theta_s$ :  $\epsilon_{-6}(\eta; \theta_s) = 1.772 \dots$

#### 4.4 Pressure as coordinates

Solving equations (17) and inserting into the formulae of sec. 4.1-4.3 yields the excess energy density as a function of the external radii  $r_j^{\text{ex}}$ ,  $j = 1, 2, 3$ . By Laplace equation (1), the curvatures are proportional to the pressure differences. If  $P_0$  denotes the pressure in the 3-cell and  $P_j$  the pressure in the neighbours  $j = 1, 2, 3$ , we can analyse as a function of the pressures.

By the scale invariance of  $\epsilon$ , we can set the absolute value of one of the external radii to 1 without loss of generality. So, fixing  $P_0 = 0$  and  $r_1^{\text{ex}} = \text{sign}(\gamma)$ , (1) implies

$$\begin{aligned} \gtrless P_1 &= \frac{\text{sign}(\gamma)}{2 \cos(\gamma + \pi/6)}; \\ \gtrless P_2 &= \frac{1}{2 r_2^{\text{ex}} \cos(\gamma + \pi/6)}; \\ \gtrless P_3 &= \frac{1}{2 r_3^{\text{ex}} \cos(\gamma + \pi/6)}; \end{aligned} \quad (33)$$

In figures 10 and 11 ( $\gamma = 6$  and  $\gamma = 6$ , respectively), we have drawn the parametric plots of the excess energy density as a function of  $P_3$  for different values of  $P_2$ .

In figure 10, the limit of  $\epsilon_{-6}(P_2; P_3)$  when  $P_3 \rightarrow 1$  corresponds to configurations of a non-symmetrical cell when the area of the 3-sided bubble goes to zero.  $P_2 = P_3 = 1$  gives the configuration "rat", whereas in all the other cases,  $P_3 \neq 1$  at fixed  $P_2$ , the bubble goes to the configuration "cat" (fig. 12).

In the Plateau border case (figure 11), when  $P_2 = P_3 = 1$ , the border goes to a configuration "fox". In the other cases,  $\epsilon_{-6}$  goes to zero. Obviously, in all cases, bubble or border, equal pressure ( $P_1 = P_2 = P_3$ ) gives  $\epsilon_{-6}(P_1; P_1) = 0$ .

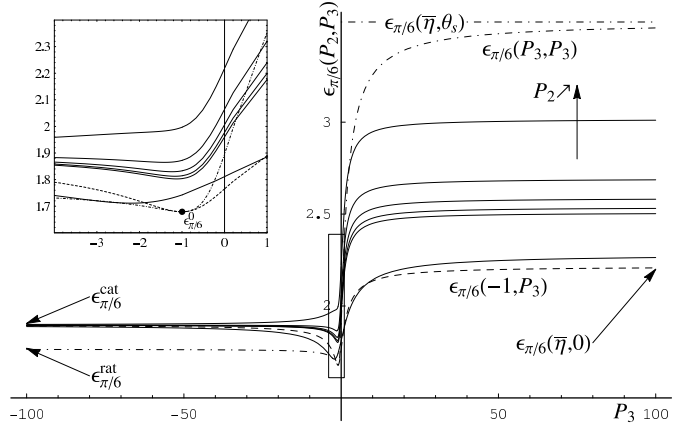


Fig. 10. Standard bubble case,  $\gamma = 6$  and  $P_1 = 1$ . Plot of  $\epsilon_{-6}$  versus the pressure  $P_3$  for different values of  $P_2$ .

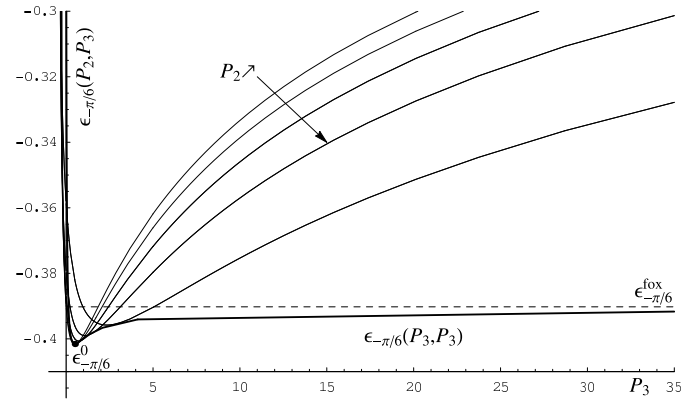


Fig. 11. Plateau border,  $\gamma = 6$  and  $P_1 = 1$ .  $\epsilon_{-6}$  is plotted with respect to  $P_3$  for different values of  $P_2$ .

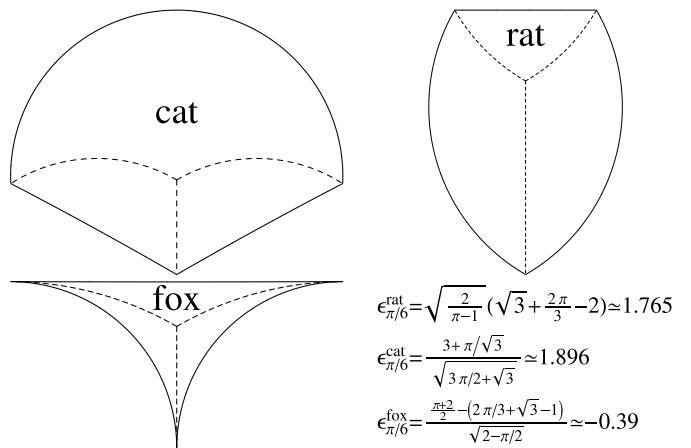


Fig. 12. Limit configurations found when one or two of the pressure differences with the neighbours go to infinity. "Rat" and "cat" describe 3-sided bubbles, while "fox" appears for Plateau borders.

#### 5 Decorating a fixed star

In this section we consider an ideal dry 2D foam at equilibrium and we ask how much the energy of the foam varies if we decorate one vertex by Plateau borders or substitut-

ing triangles. This question is important in foam rheology [8,20]. For example, in a 2D dry foam under shear, the foam response and plasticity involve topological processes triggered by vanishing edges and followed by relaxation. If the foam is not dry, the  $l_m$  length is reduced by the presence of the P lateau borders (see figure 13), favouring the switch compared to a dry foam [8]. It is well known that the yield stress of a foam decreases with the liquid fraction [21,22,23,24].

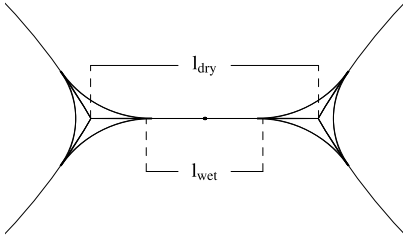


Fig. 13. The distance between two vertices in dry a foam,  $l_{\text{dry}}$ , is larger than in a wet foam,  $l_{\text{wet}}$ .

In energy term  $s$ , the presence of a P lateau border reduces the barrier that a T1 needs to overcome. Similarly, when 3-sided bubbles are inserted at some vertices of the foam, one could expect an increase of the T1 energy barrier and, therefore, a reduction of the edge tip avalanches under shear.

Varying the parameter  $q$  and fixing  $s$ , we can vary the decorating triangle area,  $\mathbb{A}^s(s; q)$ , keeping constant the internal radii  $r^{\text{in}}$ 's, that is the star. As said before, the size of the 3-cells in real foams will, in general, be smaller than the typical size of the other bubbles. In this approximation, we can write the excess energy density as a function of the triangle area. Expanding  $\mathbb{I}^{\text{ex}}$ ,  $\mathbb{I}^{\text{in}}$  and  $\mathbb{A}^s(s; q)$  with respect to  $q$ , near  $q = 0$ , we obtain

$$\mathbb{I}^{\text{ex}}(s; q) = (1 - \frac{1}{2}q^2) L_1^{\text{ex}} q + L_3^{\text{ex}} \frac{1}{2}q^2 q^3 + O(q^4); \quad (34)$$

$$\mathbb{I}^{\text{in}}(s; q) = (1 - \frac{1}{2}q^2) L_1^{\text{in}} q + L_3^{\text{in}} \frac{1}{2}q^2 q^3 + O(q^4); \quad (35)$$

$$\mathbb{A}^s(s; q) = (1 - \frac{1}{2}q^2)^2 A_2 q^2 + A_4 q^4 + O(q^5); \quad (36)$$

The coefficients of  $q^n$ , which depend only on  $s$ , are given in appendix C. Using the expansion to second order in (36) to explicit  $q$  as a function of  $\mathbb{A}^s$  and replacing this in the expression of  $\mathbb{I}^s(s; q)$ , we find:

$$s; \mathbb{A}^s = \mathbb{A}^0 + (\mathbb{A}^s) K_{\text{in}}^2(\mathbb{A}^s) \mathbb{A}^s + O(\mathbb{A}^s)^{3=2}; \quad (37)$$

where  $\mathbb{A}^0$  and  $K_{\text{in}}^2$  are given by (12) and (18), respectively. So the excess energy defined by Teixeira and Fortes [9] is, for small areas:

$$E - s; \mathbb{A}^s = \mathbb{A}^0 \mathbb{A}^{1=2} + (\mathbb{A}^s) K_{\text{in}}^2(\mathbb{A}^s) (\mathbb{A}^s)^{3=2} + O(\mathbb{A}^s)^2; \quad (38)$$

The factor  $(\mathbb{A}^s)$  in (37), (38) depends only on  $s$  and its expression is:

$$(\mathbb{A}^s) = \frac{1}{6A_2^{3=2}} \frac{L_3^{\text{ex}} L_1^{\text{ex}} A_4 = (2A_2)}{2 \cos(\theta_s = 6)} + L_1^{\text{in}} \frac{A_4}{2A_2} L_3^{\text{in}}; \quad (39)$$

Given a fixed star in a 2D dry foam, the excess energy density produced by decoration is, for small areas, linear in  $\mathbb{A}^s$ . The angular coefficient involves the numerical factor  $(\mathbb{A}^s)$ , depending on the type of the decorating 3-cell, and the star sum of the square curvatures  $K_{\text{in}}^2$ .

In particular, the excess energy density depends on  $\mathbb{A}^s$  only through the product of the triangle area and the mean square curvature of the star:

$$s; \mathbb{A}^s = \mathbb{A}^s K_{\text{in}}^2(\mathbb{A}^s); \quad (40)$$

In terms of the coordinates (31),  $\mathbb{A}^s K_{\text{in}}^2$  does not depend on  $s$ . The argument  $s$  appears only in higher order terms of the expansions of  $\mathbb{A}^s$ . In (37), the  $\mathbb{A}^{3=2}$  term is proportional to  $K_{\text{in}}^{3=2} \cos(3\theta_s)$ .

Figure 14 shows the plot of  $\epsilon_{\pi/6}(K^2 \tilde{A}_{\pi/6}, \theta_s)$  versus  $K^2 \tilde{A}_{\pi/6}$  in the case of a three-sided bubble.

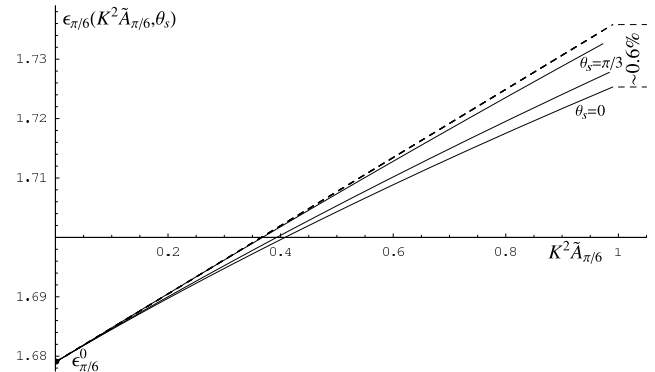


Fig. 14. The excess energy density versus  $\mathbb{A}^s K_{\text{in}}^2$  for different values of  $s$  at  $\theta_s = 6$ . Dashed, the linear approximation of  $\epsilon_{\pi/6}$ . The error for  $\mathbb{A}^s K_{\text{in}}^2 < 1$  is smaller than 0.6%.

The positive quantity  $K_{\text{in}}^2$ , depending only on  $\mathbb{A}^s$ , has the dimension of an inverse area. For a symmetrical star,  $K_{\text{in}}^2(0) = 0$ , and it increases with  $\mathbb{A}^s$ . Let us remark that, by (3), we can write:

$$K_{\text{in}}^2 = 2 (k_1)^2 k_1 k_2 + (k_2)^2; \quad (41)$$

where for simplicity we call  $k_j = 1/r_j^{\text{in}}$ . This quantity appears when 2D dry foams are studied using projective geometry and local coordinates are associated to any vertex [17].

## 6 The lower problem

The lower problem, introduced by Teixeira et al [12], consists of a dry cluster of  $n$  equal-sized bubbles surrounding

a central bubble of area  $A_c$  (fig. 15-a). By energy minimisation using Surface Evolver, the authors computed the minimal energy configurations as a function of  $A_c$ . They found that, for  $n > 6$ , the symmetrical configuration is minimal when  $A_c$  is bigger than a critical area  $A_c$ . When  $A_c < A_c$  the symmetry of the cluster is broken and the energy landscape contains multiple, but energetically equal, minima. The value of  $A_c$  corresponds to a pressure of the central bubble equal to the pressure outside the cluster.

In Cox et al.'s experimental set-up [5], the bubbles were trapped between a glass plate and the top of the liquid. The area of the central bubble was slowly decreased but the predicted symmetry breaking was not observed. Before the critical area, at some  $A_c > A_c$ , a T1 instability occurred and a bubble was ejected from the cluster. The authors explain the ejection by the presence of a small amount of liquid, which provokes the T1, and by some effects due to the third dimension.

Considering only the effect of the liquid, we estimate its influence on the occurrence of topological changes and the petal ejection. In the dry 2D model, when a  $\text{Im}$  length shrinks to zero, the unstable 4-fold vertex relaxes to a lower energy configuration where an edge joins two 3-fold vertices.

Now, with a little liquid at the vertices, the  $\text{Im}$  length is reduced by the presence of the Plateau borders, so that the topological change is likely to occur earlier. In the over, because of the Plateau borders, the  $\text{Im}$  length may vanish before the critical area  $A_c$  is reached. This is precisely confirmed by our calculations.

We have decorated over vertices by Plateau borders at constant pressure (fig. 15-b). The borders don't have the same area: by the presence of a liquid reservoir in the experimental set-up [5], the liquid area can not be fixed. Then, we calculated the value of the central area,  $A_{\text{lim}}$ , at which Plateau borders touch each other (fig. 15-c), when the ejection is conjectured to occur.

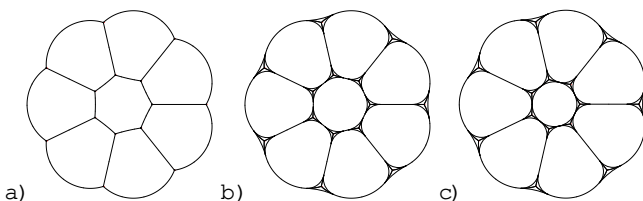


Fig. 15. Lower problem. a) The lower cluster without liquid. b) The vertices are decorated by Plateau borders. c) The limit where the Plateau borders touch each other.

Figure 16 compares the values of  $A_{\text{lim}}$  and the experimental  $A_c$  [5] as functions of  $n$ . Our values are much closer to the experimental data than those of the symmetry reduction criterion. In figure 16, the small, but systematic, difference between the ejection area and  $A_{\text{lim}}$  may be explained by considering that, experimentally, the size of the bubbles can not be exactly the same, thereby reducing the shortest  $\text{Im}$  length and triggering T1 a bit earlier than in an exactly symmetric model.

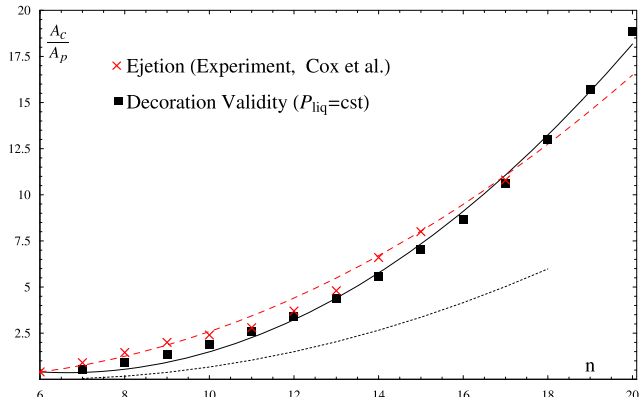


Fig. 16. Critical area of the central bubble, normalized by the petal area, versus the number of petals  $n$ . Two data sets are compared. By crosses, Cox et al.'s experiment [5], the mean critical value at which the central bubble is ejected when its area decreases. Dashed, the experimental with the largest central area at which an ejected configuration has lower energy. By squares, the calculated value at which two Plateau borders touch each other when the central area decreases at constant liquid pressure. Dotted, the theoretical curve where the lower cluster would undergo symmetry reduction.

As we don't know the experimental liquid pressure, we have chosen the liquid pressure in the Plateau borders agreeing best with the experimental points. At constant pressure, the liquid volume fraction has to vary. Figure 17 shows the predicted liquid fraction at  $A_{\text{lim}}$  as a function of  $n$ .

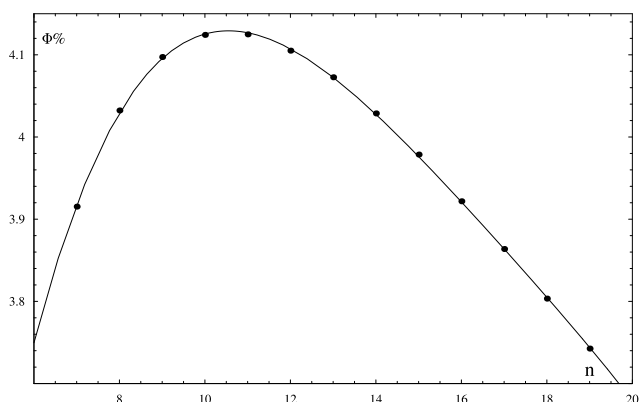


Fig. 17. Values of the liquid fraction obtained at the limit decoration versus the petal number  $n$  (fig. 16).

## 7 Conclusions

To summarise, in a 2D equilibrated foam, star-triangle equivalence permits to replace dry three-fold vertices by three-sided cells and vice versa. The general structure of a decorated star was obtained by first defining a two real parameters reference 3-cell, then applying a one complex parameter Möbius transformation. This way allowed us

to calculate all the geometrical and physical quantities of interest: area, perimeter and energy. Beside Plateau borders and standard three-sided bubbles, the method also applies to triple partitions of the disk and the three-bubble cluster.

The difference between the decorated (triangle) and bare (star) vertex is quantified by the excess energy density, which is the energy difference normalized by the square root of the triangle area. This scale invariant quantity, depending on only three parameters, serves as a shape discriminant. The most symmetric configuration minimizes.

Fixing the equilibrated star,  $\kappa$  is approximately linear as a function of the triangle area. The linear coefficient is, up to a positive factor, the mean square curvature of the star; it is zero when the star is symmetric.

As an application to the cover problem, we calculated, for various petal numbers and including liquid at the vertices, the limit value of the central area when two Plateau borders get into contact. Tuning the liquid pressure to fit the experimental data, we obtained a nice agreement of the calculated threshold with the experiment. The calculated threshold is weakly sensitive to the pressure. The small systematic difference between calculated and experimental data may be attributed to a slight discrepancy, in bubble size, of the experiment with exact n-fold symmetry.

#### Acknowledgment

We would like to thank N. Rivier and S. Cox for discussions respectively about the description of a 3-sided cell and the cover problem.

#### Appendices

##### A Möbius transformations

A Möbius transformation or homography,  $z = f(z)$ , is an automorphism of the augmented complex plane  $\mathbb{C} \cup \{\infty\}$ ,  $f : \mathbb{C} \setminus \{f^{-1}(\infty)\} \rightarrow \mathbb{C} \setminus \{f(\infty)\}$ , defined by:

$$z = f(z) = \frac{az + b}{cz + d}; \quad \text{with } ad - bc = 1; \quad (42)$$

A Möbius transformation is a combination of translations, rotations, dilatation and inversions [25].

Beside preserving angles (conformality), these transformations map circles to circles; in particular any circle passing through the inversion point,  $v = -d/c$ , is sent to a straight line (circle through infinity).

The circle of parameters  $(z_0 = 0; r) \subset \mathbb{C} \setminus \{R\}$  (centre and radius) is mapped by (42) to the circle of parameters:

$$(z_0; r) = \frac{a cr^2}{\bar{c} r^2} \frac{bd}{\bar{b} d}; \quad \frac{ad}{\bar{a} \bar{d}} \frac{bcjr}{\bar{b} \bar{c} j \bar{r}}; \quad (43)$$

where  $x$  stands for the complex conjugate of  $x$ .

Similarly,  $f$  maps the straight line of parametric equation  $z = z_0 + m t$ ,  $t \in \mathbb{R}$ , with  $z_0 = 0; m \in \mathbb{C}$ , to the circle of parameters:

$$(z_0; r) = \frac{2a \operatorname{Im}(m \bar{c} d) + i cm}{2c \operatorname{Im}(m \bar{d})}; \quad \frac{ad}{\bar{a} \bar{d}} \frac{bcj \bar{m} j}{\bar{b} \bar{c} \operatorname{Im}(m \bar{d}) j}; \quad (44)$$

When  $z_0 \neq 0$ , equations (43) and (44) keep their validity with the substitution:  $b \mapsto b + az_0$  and  $d \mapsto d + cz_0$ .

#### B 3-cell perimeters

Let us consider a edge defined by its parametrization  $\gamma(u)$ ,  $u \in [u_0; u_1]$ . In the transformed plane, the length of  $\gamma = f_s$ , in age of  $\gamma$  by  $f_s$ , is

$$\begin{aligned} \int_{u_0}^{u_1} \|\gamma'(u)\| du &= \int_{u_0}^{u_1} \frac{\partial f_s}{\partial z}(\gamma(u)) \gamma'(u) du = \\ &= (1 - \frac{\bar{b} \bar{f}}{\bar{a} \bar{f}}) \int_{u_0}^{u_1} \frac{1}{\|\gamma'(u)\|^2} \gamma'(u) du; \end{aligned} \quad (45)$$

##### B.1 Internal perimeter

For an internal line  $\gamma_j^{\text{in}}(t)$ , substituting equation (7) in (45) gives, after simplification:

$$\begin{aligned} \int_j^{\text{in}} &= (1 - \frac{\bar{b} \bar{f}}{\bar{a} \bar{f}}) \int_0^{\frac{\pi r}{3}} \frac{du}{1 - 2u \bar{b} \bar{f} \cos(s - j) + u^2 \bar{b} \bar{f}} \\ &= \kappa_j^{\text{in}}(s) \kappa_j^{\text{in}}(s; q); \end{aligned} \quad (46)$$

where  $\kappa_j^{\text{in}}(s; q)$  is given in (21).

##### B.2 External perimeter

For an external edge  $\gamma_j^{\text{ex}}(t)$ , (45) can be reduced to an integral of the form:

$$\int_j^{\text{ex}} = \frac{q(1 - \bar{b} \bar{f})}{2 \bar{b} \sin(j)} \int_1^{\frac{\pi}{3}} \frac{du}{a_0^j + a_1^j \cos(u) + a_2^j \sin(u)}; \quad (47)$$

where the constants in the integral are:

$$\begin{aligned} a_0^j &= 1 + \frac{\bar{b} \bar{f} q}{3} \cos(j - s) (1 - \frac{p}{3} \cot(j)) + \\ &+ \frac{\bar{b} \bar{f} q^2}{12 \sin^2(j)} (5 + 2 \cos(2j - \pi/3)); \end{aligned} \quad (48)$$

$$\begin{aligned} a_1^j &= \frac{\bar{b} \bar{f} q}{\sin(j - s)} + \\ &+ \frac{\bar{b} \bar{f} q^2 (1 - \frac{p}{3} \cot(j))}{2 \frac{p}{3} \sin(j)}; \end{aligned} \quad (49)$$

$$a_2^j = \frac{\bar{b} \bar{f} q \sin(j - s)}{\sin(j)}; \quad (50)$$

they verify

$$(a_0^j)^2 - (a_1^j)^2 - (a_2^j)^2 = \frac{q^2 (1 - \beta_j^2)^2}{4 (r_j^{\text{ex}})^2 \sin^2} > 0 : \quad (51)$$

The solution of the integral (47), verifying (51), is [27]:

$$r_j^{\text{ex}} = \frac{q (1 - \beta_j^2)}{j \sin j} \frac{6}{4} \frac{\arctan \frac{(a_0^j a_1^j) \tan(u=2) + a_2^j}{(a_0^j)^2 (a_1^j)^2 (a_2^j)^2}}{q \frac{7}{5}} : \quad (52)$$

Summing (52) over  $j$ , we get:

$$r^{\text{ex}} = r_j^{\text{ex}} (s; q; ) \frac{1}{h} \frac{r_j^{\text{ex}} (s; q; )}{2 r_j^{\text{ex}} \arctan 2 r_j^{\text{ex}} \sin \frac{(a_0^j a_1^j) \tan(u=2) + a_2^j}{q (1 - \beta_j^2)}} : \quad (53)$$

Equation (53) also defines the angle  $\beta_j^{\text{ex}}$  subtended by the external edge  $\gamma_j^{\text{ex}}$ .

## C Series coefficients of

The coefficients in the expressions (34), (35) and (36) are:

$$\begin{aligned} L_1^{\text{in}} &= \frac{p}{3}; & L_3^{\text{in}} &= \frac{1}{3^3 3}; & L_1^{\text{ex}} &= \frac{1}{\sin}; \\ L_3^{\text{ex}} &= \frac{\frac{p}{3} + 5}{4} \frac{2 \frac{p}{3} \sin(2 + \pi/6)}{4 \sin^3( )}; \\ A_2 &= \frac{1}{4 \sin} \frac{3}{\sin} \frac{2}{\cos( + \pi/6)}; \\ A_4 &= \frac{1}{8} \left( 4 \left( \frac{p}{3} \right) + (9 + 4 \frac{p}{3}) \cot \csc^2 + \right. \\ &\quad \left. + \frac{9}{8} \csc^4 - \frac{1}{4^2 3} (1 + \frac{p}{3} \cot) \right); \end{aligned}$$

The zeroth and second order (in  $q$ ) coefficients of  $r^{\text{ex}}$  and  $r^{\text{in}}$  are zero at  $q = 0$ . In the same way  $A_0, A_1$  and  $A_3$  are zero.

## References

1. J.A. F. Plateau, *Statique expérimentale et théorique des liquides soumis aux seules forces moléculaires*, (Gauthier-Villars, Paris, 1873).
2. D. Weaire and S. Hutzler, *The physics of foams* (Clarendon Press, Oxford, 1999).
3. M. Mancini and C. Oguey, *Phil. Mag. Lett.* 83, 643–649 (2003).
4. J. Stavans and J.A. Glazier, *Phys. Rev. Lett.* 62, 1318 (1989).
5. S.J. Cox, M.F. Vaz and D. Weaire, *Eur. Phys. J. E* 11, 2935 (2003).
6. M.F. Vaz and S.J. Cox and M.D. Alonso, *J. Phys.: Condens. Matter* 16, 4165 (2004).
7. F. Bolton and D. Weaire, *Phil. Mag. B* 63, 795 (1991), 65, 437 (1992).
8. Qicheng Sun, Stefan Hutzler, *Coll. Surf. A* 263, 27–32 (2005).
9. P.I.C. Teixeira and M.A. Fortes, *Phil. Mag.* 85, 1303–1322 (2005).
10. M. Mancini and C. Oguey, *Coll. Surf. A* 263, 33–38 (2005).
11. F.T. Lewis, *Am. Nat. Rec.* 38, 341 (1928).
12. D. Weaire, S.J. Cox, F. Graner, *Eur. Phys. J. E* 7, 123 (2002).
13. C. Moukarzel, *Phys. Rev. E* 55, 6866–6880 (1997).
14. A. Neimark and M. Vignes-Adler, *Phys. Rev. E* 51, 788 (1995).
15. G.B. Han, A. Dussaud, B. Brunet-Foch, A.V. Neimark and M. Vignes-Adler, *J. Non-Equilibrium Thermodyn.* 25, 325 (2000).
16. D. Weaire, *Phil. Mag. Lett.* 79, 491–495 (1999).
17. M. Mancini, PhD Thesis, Université de Cergy-Pontoise (France, 2005). <http://tel.ccsd.cnrs.fr/tel-00010304>.
18. P.I.C. Teixeira and M.A. Fortes, *Phys. Rev. E* 71, 51404 (2005) and talk T33 at Eurofoam 2006, July 2–6, Potsdam D.
19. A. Cárcole and M. Ritoré, *Ind. Univ. Math. J.* 53/3, 883–904 (2004).
20. D. Weaire, S. Hutzler, S. Cox, N. Kern, M.D. Alonso and W. Drenckhan, *J. Phys.: Condens. Matter* 15, S65–S73 (2003).
21. T.G. Mason, J. Bibette, D.A. Weaire, *J. Colloid Interface Sci.* 179 (1996) 439.
22. B.S. Gardiner, B.Z. Dlugogorski, G.J. Jamison, R.P. Chhabra, *J. Rheol.* 42 (1998) 1437.
23. A. Saint-Jalmes and D.J. Durian, *J. Rheol.* 43, 6, 1411–1422 (1999).
24. F. Rouyer, S. Cohen-Addad and R. Hohler, *Coll. Surf. A* 263, 111–116 (2005).
25. Z. Nehari, *Conformal mapping*, (New York, McGraw-Hill, 1952).
26. B.A. Dubrovin, A.T. Fomenko, S.P. Novikov, *Modern geometry – methods and applications. Part 1. The geometry of surfaces, transformation groups, and fields*, (Springer-Verlag, Berlin, 1992).
27. I.M. Ryshik and I.S. Gradshteyn, *Tables of Series, Products, and Integrals* (VEB Deutscher Verlag der Wissenschaften, Berlin, 1963).

